Available online at www.sciencedirect.com
SCIENCE DIRECT®
International Journal of Solids and Structures 42 (2005) 2225–2241
INTERNATIONAL JOURNAL OF SOLIDS and STRUCTURES
www.elsevier.com/locate/ijsolstr

On forming limit stress diagram analysis

P.D. Wu [a,*], A. Graf [a], S.R. MacEwen [a], D.J. Lloyd [a], M. Jain [b], K.W. Neale [c]

[a] *Alcan International Limited, Kingston Research & Development Centre, Kingston, Ont., Canada K7L 5L9*
[b] *Department of Mechanical Engineering, McMaster University, Hamilton, Ont., Canada L8S 4L7*
[c] *Faculty of Engineering, University of Sherbrooke, Sherbrooke, Que., Canada J1K 2R1*

Received 2 June 2004; received in revised form 14 September 2004
Available online 27 October 2004

Abstract

Forming Limit Stress Diagrams (FLSDs) have been intensively studied and have been considered as being path-independent. This paper carries out a detailed study to examine the path-dependency of FLSDs based on different non-proportional loading histories, which are combinations of two linear strain paths. All simulations are based on crystal plasticity theory in conjunction with the M–K approach. It is confirmed that the Forming Limit Diagram (FLD) and the FLSD are two mathematically equivalent representations of forming limits in strain-space and stress-space, respectively. While the FLD is very sensitive to strain path changes, the FLSD is much less path-dependent. It is suggested that the FLSD is much more favourable than the FLD in representing forming limits in the numerical simulation of sheet metal forming processes. The nature of the effect of a strain path change on forming limits is investigated in terms of the transition work hardening behaviour upon the path change, and the concept of the FLSD.

Keywords: Sheet metal; Formability; Crystal plasticity

1. Introduction

Great efforts have been made to reduce weight and increase fuel-efficiencies in automobiles by gradually increasing the usage of aluminium alloys. However, the formability of aluminium alloys is often viewed as inferior to that of steel, which is still the dominant materials in automotive body panels. Very intensive research has been carried out on understanding the effects of material microstructures and textures on the formability of aluminium sheet. In most of these investigations, the concept of the Forming Limit Diagram (FLD) has been used to represent conditions for the onset of sheet necking (see e.g. Hecker, 1975); this is

* Corresponding author. Tel.: +1 613 5412082; fax: +1 613 5412134.
E-mail address: pei-dong.wu@alcan.com (P.D. Wu).

0020-7683/$ - see front matter © 2004 Elsevier Ltd. All rights reserved.
doi:10.1016/j.ijsolstr.2004.09.010

now a standard tool for characterising materials in terms of their overall forming behaviour. However, experimentally measuring an FLD is a very time consuming procedure, and the scatter in experimental data for a given sheet is often so large that researchers sometimes question the accuracy and precision with which the FLD has been determined (see e.g. Janssens et al., 2001). As a result, a significant effort has been spent on developing more accurate and reliable numerical procedures to construct FLDs, while experimental procedures for measuring FLDs constantly improve.

Most theoretical and numerical FLD analyses have been based on the so-called M–K approach, developed by Marciniak and Kuczynski (1967). The basic assumption of this approach is the existence of a material imperfection, in the form of a groove on the surface of the sheet. They showed that a slight intrinsic inhomogeneity in load bearing capacity throughout a deforming sheet can lead to unstable growth of strain in the region of the imperfection, and subsequently cause localized necking and failure. Within the M–K framework, the influence of various constitutive features on FLDs has been explored using phenomenological plasticity models (see e.g. Neale and Chater, 1980) and crystal plasticity (see e.g. Zhou and Neale, 1995; Wu et al., 1997). Furthermore, the FLD also has been used to evaluate analytical yield functions for anisotropic sheets (see e.g. Wu et al., 2003). Using the M–K approach, the predicted FLDs based on crystal plasticity were in good agreement with measured FLDs for rolled aluminium alloy sheets (Wu et al., 1998b; Knockaert et al., 2002).

However, both experimental and numerical results have indicated that FLDs are very sensitive to strain path changes (see e.g. Laukonis and Ghosh, 1978; Graf and Hosford, 1993, 1994; Zhao et al., 1996; Hiwatashi et al., 1998; Wu et al., 1998a; Kuroda and Tvergaard, 2000). There is no single curve in strain space that represents the forming limit, and this limits the use of conventional FLDs for assessing forming severity because the straining path of material elements in a real sheet metal forming process is usually not known with any certainty. Therefore, finding a single path-independent curve to characterize forming limits is of considerable practical interest. Knowing the drawback of conventional FLDs, Arrieux et al. (1982), among others, represented formability based on the state of stress rather than the state of strain. They constructed a Forming Limit Stress Diagram (FLSD) by plotting the calculated principal stresses at necking. It was concluded that all FLSDs, based on phenomenological plasticity models such as Hill (1948) and Hosford (1979), were almost path-independent (Arrieux, 1995; Zhao et al., 1996; Haddad et al., 2000; Stoughton, 2000; Zimniak, 2000; Stoughton and Zhu, 2004). In a preliminary study on the FLSD based on crystal plasticity, Wu et al. (2000) came to a similar conclusion. In these studies, non-proportional loading histories were developed using combinations of two linear strain paths. The first strain path, the pre-strain operation, was common to all loading histories. Subsequent linear deformation paths were imposed by varying the strain-rate ratio for the development of an FLD applicable to that given pre-strain path and amount. However, the amount of pre-straining was relatively small in the sense that it was well below the FLD for linear proportional strain paths. It is important to assess the path-dependency of the FLSD when pre-strains are very large. Furthermore, previous research concentrated on constructing the FLSD and confirming that the FLSD was indeed insensitive to strain path changes. However, it is equally important to verify whether the path-dependent nature of the forming limit curves in strain space can be reproduced by directly mapping points on the stress-based limit curve to strain for a given loading history. In addition, it seems that the FLSD itself could be used to explain the nature of the effect of a strain path change on forming limits.

This paper re-examines the path-dependency of the forming limit stress diagram based on different non-proportional loading histories, which are combinations of two linear strain paths. All simulations are based on the numerical procedure developed by Wu et al. (1997), in which the Asaro and Needleman (1985) polycrystal plasticity model, in conjunction with the M–K approach, is used to calculate the FLDs for FCC polycrystals. The nature of the effect of a strain path change on forming limits is investigated in terms of the influence of pre-straining on the stress–strain curves for subsequent strain paths and the concept of the FLSD.

2. Constitutive model

The constitutive model is based on the rate-dependent crystal plasticity model formulated by Asaro and Needleman (1985) and employed by Wu et al. (1996). This model allows for slip system hardening as well as lattice elasticity. It leads to a constitutive relation of the following form for each grain:

$$\overset{\nabla}{\boldsymbol{\sigma}} = \boldsymbol{L}\boldsymbol{D} - \dot{\boldsymbol{\sigma}}^0 - \boldsymbol{\sigma}\,\mathrm{tr}\,\boldsymbol{D} \tag{1}$$

where $\overset{\nabla}{\boldsymbol{\sigma}}$ denotes the Jaumann rate of the Cauchy stress tensor, $\boldsymbol{L}$ is the tensor of elastic moduli, $\boldsymbol{D}$ represents the strain-rate tensor, and $\dot{\boldsymbol{\sigma}}^0$ accounts for the visco-plastic type stress rate that is determined by the slip rates on the various slip systems in the crystal. The slip rates are governed by the power-law expression

$$\dot{\gamma}_\alpha = \dot{\gamma}_0 \,\mathrm{sgn}\,\tau_\alpha \left|\frac{\tau_\alpha}{g_\alpha}\right|^{1/m} \tag{2}$$

where $\dot{\gamma}_0$ is a reference shear rate taken to be the same for all slip systems, τ_α is the resolved shear stress on slip system α, g_α is its hardness and m is the strain-rate sensitivity index. In the present study, isotropic hardening will be assumed and results will be given for a slip system strength law of the power-law form

$$\dot{g}_\beta = h_0 \left(\frac{h_0 \gamma_a}{\tau_0 n} + 1\right)^{n-1} \tag{3}$$

where τ_0 is an initial critical shear stress, h_0 is the system's initial hardening rate, n is the hardening exponent and γ_a is the accumulated slip.

The response of a polycrystal comprised of many grains is obtained by invoking the Taylor assumption. Thus, at a material point representing a polycrystal of many grains, the deformation in each grain is taken to be identical to the macroscopic deformation of the continuum. Furthermore, the macroscopic values of all quantities, such as stresses, stress rates and elastic moduli, are obtained by averaging their respective values over the total number of grains at the particular material point.

3. Problem formulation and method of solution

The constitutive model outlined above is implemented, in conjunction with the M–K approach, into a numerical code to predict FLDs for polycrystalline sheets having orthotropic textures. The axes x_1 and x_2 define the rolling direction (RD) and the transverse direction (TD) in the plane of the sheet, while x_3 represents the direction normal to the sheet (ND).

The basic assumption of the M–K approach is the existence of initial material or geometric imperfections in the form of a groove or band that is initially inclined at an angle ψ_I with respect to the x_1 reference direction (Fig. 1). Quantities inside the band are denoted by $(\,)^{\mathrm{b}}$. The thickness along the minimum section in the band is denoted by $h^{\mathrm{b}}(t)$, with an initial value $h^{\mathrm{b}}(0)$. The initial geometric non-uniformity is defined by

$$f = \frac{h^{\mathrm{b}}(0)}{h(0)} \tag{4}$$

with $h(0)$ being the initial sheet thickness outside the imperfection groove.

The deformation outside the imperfection band is assumed to be either "strain controlled" or "stress controlled". In the strain controlled case, we assume:

$$\frac{D_{22}}{D_{11}} = \frac{\dot{\varepsilon}_{22}}{\dot{\varepsilon}_{11}} = \rho, \quad D_{12} = 0, \quad W_{12} = 0 \tag{5}$$

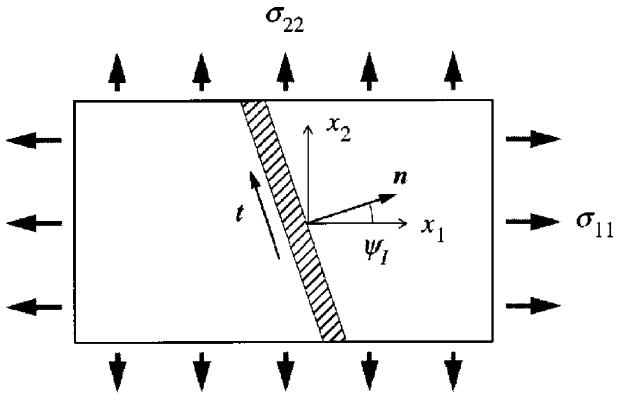

Fig. 1. The geometry and the convention employed in the FLD analysis.

where $\dot{\varepsilon}_{22} = D_{22}$ and $\dot{\varepsilon}_{11} = D_{11}$ are the (principal) logarithmic strain rates and the W_{ij} values are components of the spin tensor. In the stress controlled case, we have

$$\frac{\dot{\sigma}_{22}}{\dot{\sigma}_{11}} = \alpha, \quad \dot{\sigma}_{12} = 0 \tag{6}$$

It is further assumed, in both cases, that $D_{13} = D_{23} = W_{13} = W_{23} = 0$, while D_{33} is specified by the condition $\dot{\sigma}_{33} = 0$. For the orthotropic textures considered here, these boundary conditions imply that the average stress components $\sigma_{13} = \sigma_{23} = 0$. It is appropriate to define some important strain paths in terms of the strain ratio ρ and stress ratio α as follows:

- uniaxial tension: $\alpha = 0$,
- uniaxial stretching: $\rho = -0.5$,
- in-plane plane strain tension: $\rho = 0$,
- equi-biaxial tension: $\alpha = 1$,
- equi-biaxial stretching: $\rho = 1$.

Under the imposed deformations described in (5) and (6), the evolution of the groove orientation ψ is given by

$$\dot{\psi} = n_1 n_2 (D_{11} - D_{22}) - n_1^2 D_{12} \tag{7}$$

where $n_1 = \cos\psi$ and $n_2 = \sin\psi$ are the components of the unit normal to the band in the current configuration (Fig. 1).

Apart from the necessary conditions at the band interface, equilibrium and compatibility inside and outside the band are automatically satisfied because uniform deformations are assumed both inside and outside the band. The compatibility condition at the band interface is given in terms of the differences in the velocity gradients inside and outside the band:

$$L^{\mathrm{b}}_{\alpha\beta} = L_{\alpha\beta} + v_\alpha n_\beta \tag{8}$$

or

$$D^{\mathrm{b}}_{\alpha\beta} = D_{\alpha\beta} + \frac{1}{2}(v_\alpha n_\beta + n_\alpha v_\beta), \quad W^{\mathrm{b}}_{\alpha\beta} = W_{\alpha\beta} + \frac{1}{2}(v_\alpha n_\beta - n_\alpha v_\beta) \tag{9}$$

where v_α are parameters to be determined. Here, and subsequently, Greek indices range from 1 to 2. Equilibrium balance on each side of the interface requires that

$$n_\alpha \sigma^{\mathrm{b}}_{\alpha\beta} h^{\mathrm{b}} = n_\alpha \sigma_{\alpha\beta} h \tag{10}$$

in the current configuration. A set of incremental equations for v_α is now obtained by substituting the incremental constitutive equation (1) into the incremental form of (10), using (9) to eliminate the strain increments $D^{\mathrm{b}}_{\alpha\beta}$. Together with the condition $\dot{\sigma}^{\mathrm{b}}_{33} = 0$, this furnishes three algebraic equations for solving v_1, v_2 and the unknown D^{b}_{33}.

The solution is obtained numerically by a linear incremental procedure. At any given stage of the prescribed deformation path, the moduli $\boldsymbol{L}$ and $\dot{\boldsymbol{\sigma}}^0$ in (1) are calculated for all grains inside and outside the band, by updating from the previous increment. The corresponding moduli and the visco-plastic type stress rates for the polycrystals representing materials inside and outside the band are obtained by averaging over all grains inside and outside the band, respectively. Therefore, the rates v_α, or $D^{\mathrm{b}}_{\alpha\beta}$, and D^{b}_{33} inside the band are directly calculated by solving the three above-mentioned algebraic equations. The sheet thickness outside the band h and inside the band h^{b} are updated based on the relations

$$\dot{h} = D_{33} h, \quad \dot{h}^{\mathrm{b}} = D^{\mathrm{b}}_{33} h^{\mathrm{b}} \tag{11}$$

The onset of sheet necking is defined by the occurrence of a much higher maximum principal logarithmic strain rate inside the band than outside, taken here as the condition $\dot{\varepsilon}^{\mathrm{b}}/D_{11} \geqslant 10^5$, where $\dot{\varepsilon}^{\mathrm{b}}$ represents the strain rate inside the band. The corresponding principal logarithmic strains ε^*_{11} and ε^*_{22}, and principal stresses σ^*_{11} and σ^*_{22} outside the band are the limit strains and limit stresses respectively. For a real sheet, numerous initial imperfections can exist with different orientations. A conservative estimate of the forming limit strain is that obtained from limit strain values for various values of the initial groove orientation ψ_I, and then selecting the minimum value as the actual forming limit strain. The entire FLD of a sheet is determined by repeating the procedure for different strain paths outside the band as prescribed by the strain-rate ratio ρ or stress-rate ratio α. The non-proportional loading histories are developed using combinations of two linear strain paths. The first strain path, the pre-strain operation, is common to all loading histories. Subsequent linear deformation paths are imposed by varying the strain-rate ratio for the development of an FLD applicable to that given pre-strain path and amount.

It is to be noted that, since the deformations inside and outside the band are assumed to be homogeneous, the rather complex polycrystal plasticity model need only be applied to two separate stress–strain histories, one inside and one outside the band. Therefore, the computational requirements are relatively modest.

4. Results

The sheet considered here is an aluminium alloy AA6111-T4. Fig. 2 shows the initial texture represented by the {1 1 1} pole figure. The values for the material parameters in the crystal plasticity analysis are $C_{11} = 236\,\mathrm{GPa}$, $C_{12} = 135\,\mathrm{GPa}$ and $C_{44} = 62\,\mathrm{GPa}$, $\dot{\gamma}_0 = 0.001\,\mathrm{s}^{-1}$, $m = 0.002$, $\tau_0 = 47\,\mathrm{MPa}$, $h_0/\tau_0 = 30$, $n = 0.23$ and $q = 1.0$. It is noted that the crystal elastic constants, the strain rate sensitivity m and the slip system reference plastic shearing rate $\dot{\gamma}_0$ are typical for an aluminium sheet. The hardening parameters are estimated by curve-fitting numerical simulations of uniaxial tension in the RD to the corresponding experimental data. Fig. 3 shows that the curve fitting is quite good. Furthermore, the value of the initial imperfection parameter was taken as $f_0 = 0.992$, which was determined by fitting the FLD prediction of in-plane plane strain tension ($\rho = 0$) to the corresponding experimental limit strain for the sheet as-received.

For simplicity, in all figures, the limit strains are denoted by ε_{11} and ε_{22} instead of ε^*_{11} and ε^*_{22}. Similarly, the limit stresses σ^*_{11} and σ^*_{22} are replaced by σ_{11} and σ_{22}.

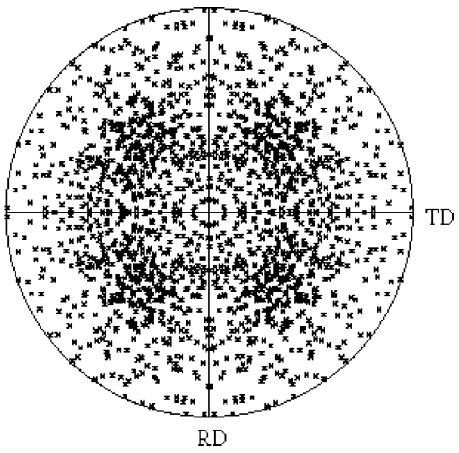

Fig. 2. Initial texture represented by the {111} pole figure.

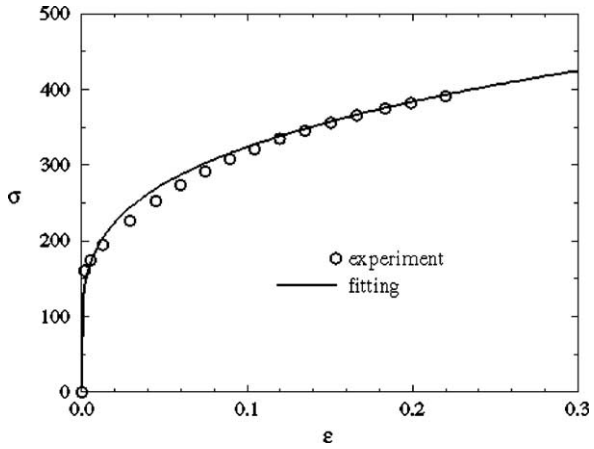

Fig. 3. Tensile stress–strain response in uniaxial tension along the RD for as-received AA6111-T4.

Fig. 4 shows the measured and predicted FLDs for the as-received sheet. In general, the agreement between the experiments and simulations is quite good. The predicted forming limit stress diagram is presented in Fig. 5. In this figure the limit stresses at necking are calculated for linear strain paths in the range of $(-0.9 < \rho < 1.2)$, and for linear stress paths $(0 < \alpha < 1)$. It is found that the limit stress curves, based respectively on linear strain and linear stress paths, are reduced to a single curve, which defines the Forming Limit Stress curve (FLSc) or simply FLSD for the sheet.

Fig. 6 gives the predicted limit stresses under non-proportional loading histories, shown as different symbols in the figure. The non-proportional loading histories are combinations of two linear paths. The first loading path, the pre-straining operation, is common to all loading histories and is stress or strain controlled. Assuming ε_{11} and ε_{22} to be the strain components at the end of pre-straining, the effective pre-strain is defined as $\varepsilon_e = 2\sqrt{(\varepsilon_{11}^2 + \varepsilon_{11}\varepsilon_{22} + \varepsilon_{22}^2)/3}$ (i.e., the von Mises effective strain under the assumption of material incompressibility). Subsequent linear strain paths are imposed by varying the strain-rate ratio (ρ) for the development of an FLD applicable to the given pre-straining path and amount. For example, the legend "$\alpha = +0.0$ $(-0.043, 0.10)$" indicates that the sheet is pre-strained in uniaxial tension along the RD up to

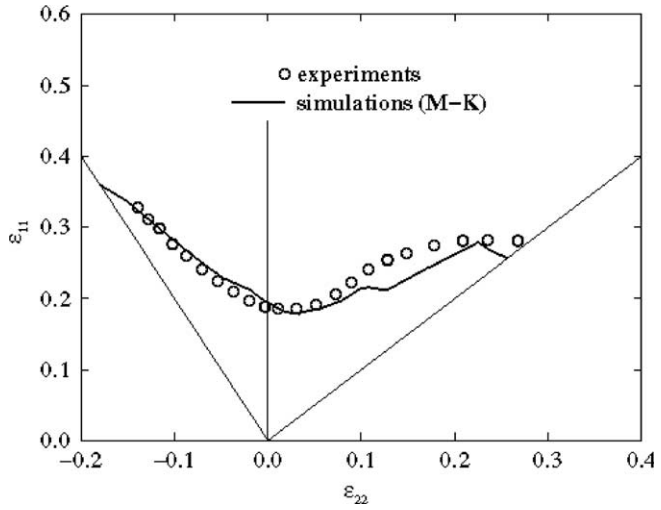

Fig. 4. Predicted and measured FLDs for as-received AA6111-T4.

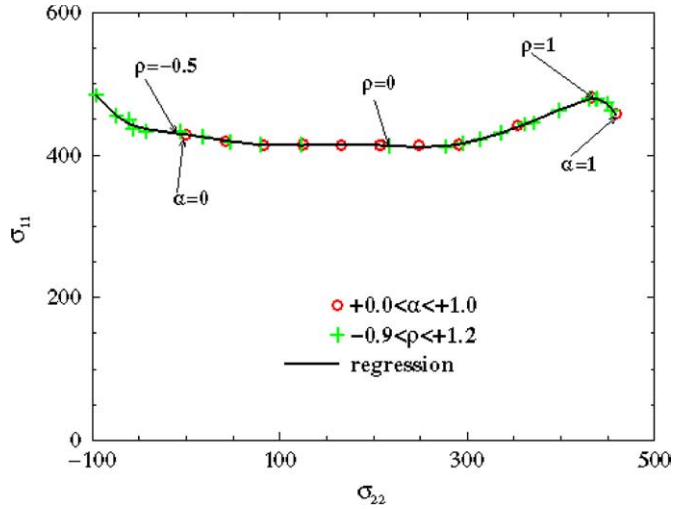

Fig. 5. Predicted FLSD under proportional deformation paths.

$\varepsilon_{22} = -0.043$ and $\varepsilon_{11} = 0.10$. It is found that, if the amount of pre-strain is not very large, the predicted limit stresses under non-proportional loading histories form a very narrow band around the FLSc [the FLSD based on linear loading paths (Fig. 6a)]. Under large pre-straining (Fig. 6b) the predicted limit stresses are still close to the FLSc, except for the *worst* case in which the pre-straining is equi-biaxial tension ($\alpha = 1$) ending at $\varepsilon_{22} = 0.252$ and $\varepsilon_{11} = 0.20$ ($\varepsilon_{22} \neq \varepsilon_{11}$ due to the material anisotropy). Knowing that the limit strains under equi-biaxial tension are $\varepsilon_{22} = 0.288$ and $\varepsilon_{11} = 0.228$ for the as-received sheet, it is found that the pre-straining in the worst case nearly reaches the forming limit. The effective pre-strain is about 0.45 in the worst case, and about 0.20 for the other cases shown in Fig. 6b, compared with about 0.1 for the cases in Fig. 6a.

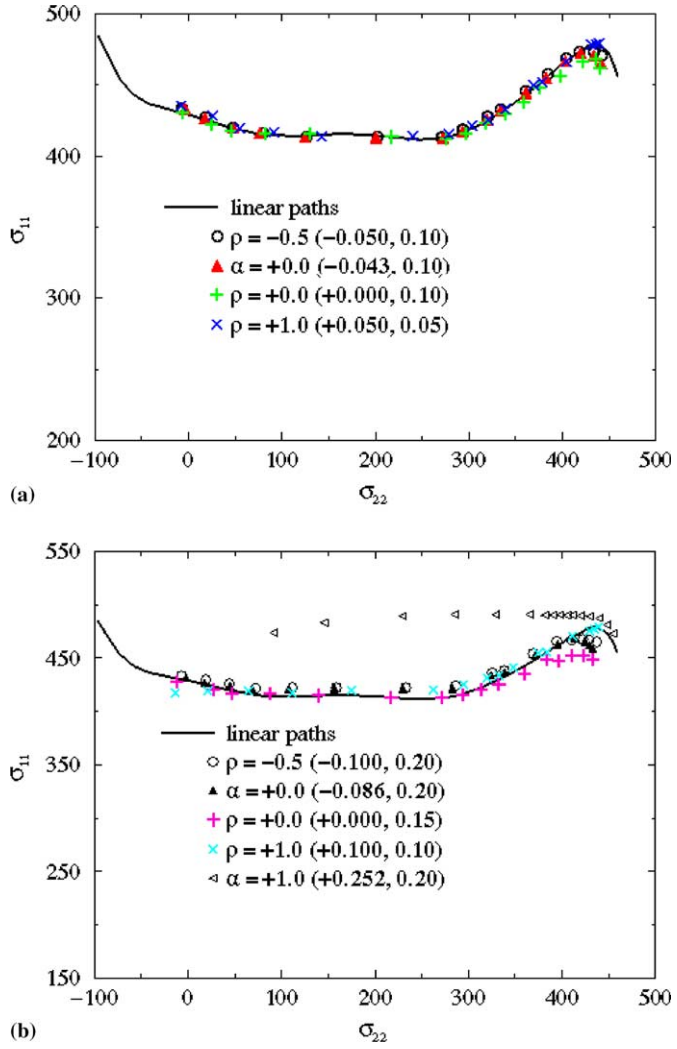

Fig. 6. Predicted limit stresses for the sheet pre-strained to different levels: (a) about $\varepsilon_e = 0.1$ and (b) $\varepsilon_e \geqslant 0.2$ in various different pre-straining paths indicated by different symbols.

From results shown in Fig. 6, it is clear that the limit points under non-proportional loadings are almost on the FLSc (for linear deformation paths) if the pre-strains are not too large. Even when the pre-straining is very large, the predicted limit stresses are still not far away from the FLSc. Therefore, the forming limit stress diagram is not very sensitive to strain path changes, especially when compared to the path-dependence in the FLDs as shown in Wu et al. (1998b). If the FLSD is assumed to be path-independent, it is interesting to consider whether the FLSD can be used to calculate the path-dependent FLD.

Considering first the effect of uniaxial stretching ($\rho = -0.5$) on forming limits, the constitutive equation (1) is first integrated along the strain path of uniaxial stretching up to a certain level of strain ε_{11}, and then along another linear strain path ($\rho = \text{const}$). The simulation is terminated when the computed stresses hit the FLSD, and the corresponding in-plane strain components are considered as the limit strains, which form a point in the FLD. The entire FLD is determined by repeating the procedure for different strain paths

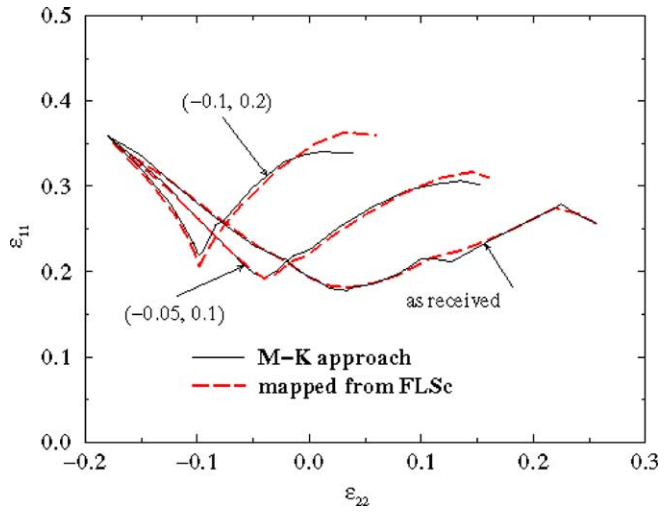

Fig. 7. Predicted FLDs for the sheet pre-strained to different levels in uniaxial stretching ($\rho = -0.5$).

as prescribed by the strain-rate ratio ρ ($-0.5 \leqslant \rho \leqslant 1.0$). Fig. 7 shows FLDs for both the as-received and sheets pre-strained in uniaxial stretching up to $\varepsilon_{11} = 0.1$ and 0.2, respectively. For a comparison, the FLDs based on the M–K approach are also included in Fig. 7. It is clear from Fig. 7 that the effect of uniaxial stretching on the FLD based on the M–K approach is reproduced by directly mapping the FLSD into strain-space. More specifically, pre-straining slightly increases the major limit strain ε_{11} for in-plane plane strain tension, but significantly enhances the limit strain ε_{11} for equi-biaxial stretching. These are in good agreement with the experimental observations of Graf and Hosford (1994). For the as-received sheet, results based on the two approaches are almost identical. The very small difference is due to the fact that

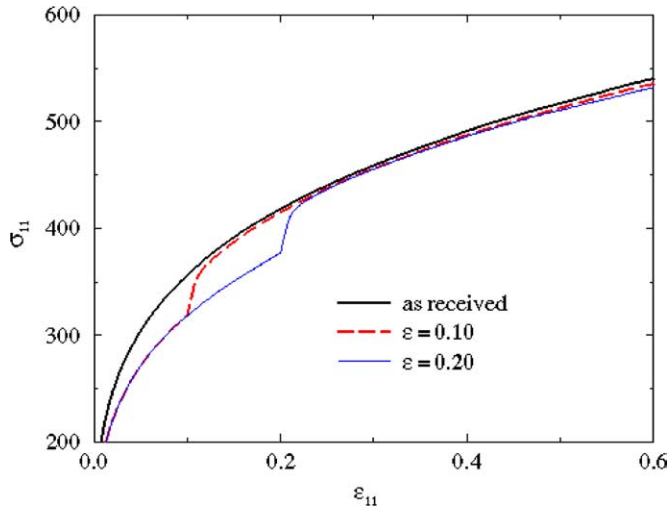

Fig. 8. Calculated σ_{11} vs. ε_{11} curves under in-plane plane strain tension after the sheet is pre-strained to different levels in uniaxial stretching ($\rho = -0.5$).

the FLSD is a smooth curve, which is a regression of the discrete limit stresses. For the pre-strained sheets, noticeable differences are found only in strain paths near equi-biaxial tension.

As mentioned previously, the mechanism that alters the FLD due to strain path changes may be studied by observing, in view of the concept of the FLSD, the effect of the pre-straining on the stress–strain curves in subsequent strain paths. This can mainly be done in terms of the influence of pre-straining on σ_{11} vs. ε_{11} and/or σ_{11} vs. ε_{22} curves, because the forming limit stress σ_{11}^{*} is almost a constant for a large portion of the FLSc (see Fig. 5). Fig. 8 presents the stress σ_{11} vs. strain ε_{11} curves for both the as-received and sheets pre-strained in uniaxial stretching up to $\varepsilon_{11} = \varepsilon = 0.1$ and 0.2, respectively. It is clear that the pre-straining very slightly decreases the

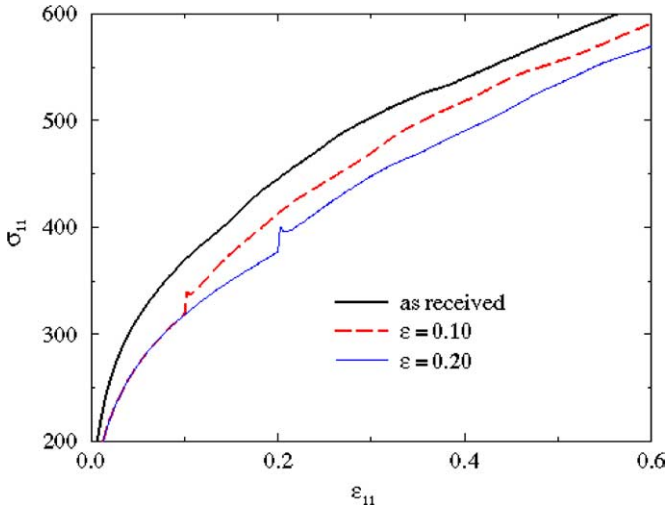

Fig. 9. Calculated σ_{11} vs. ε_{11} curves under equi-biaxial stretching after the sheet is pre-strained to different levels in uniaxial stretching ($\rho = -0.5$).

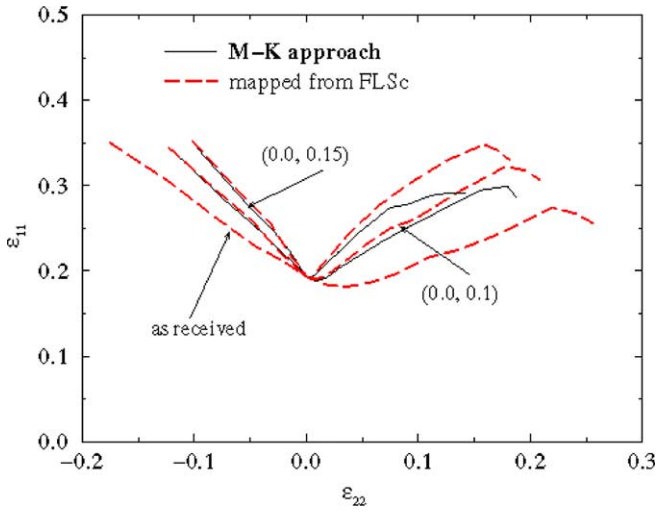

Fig. 10. Predicted FLDs for the sheet pre-strained to different levels in in-plane plane strain tension ($\rho = 0$).

flow stress σ_{11} in subsequent in-plane plane strain tension. This implies that the pre-straining will slightly delay the subsequent in-plane plane strain tension state hitting the FLSD. As a result, the pre-straining slightly increases the major limit strain ε_{11} for in-plane plane strain tension. Fig. 9 indicates that the uniaxial stretching pre-straining significantly decreases the flow stress σ_{11} in subsequent equi-biaxial stretching. Therefore, the pre-straining significantly increases the limit strain ε_{11} in equi-biaxial stretching.

The effect of in-plane plane strain tension ($\rho = 0$) on the FLD is presented in Fig. 10. As expected, the limit strain for in-plane plane strain tension is not affected by the pre-straining. The FLD shape changes from U towards V due to the pre-straining. For uniaxial stretching, it is found that the pre-straining has almost no effect on the limit strain ε_{11}, but it dramatically decreases the limit strain ε_{22}. This observation could be explained by Fig. 11, which gives the effect of in-plane plane strain tension on subsequent uniaxial stretching in terms of the σ_{11} vs. ε_{11} and σ_{11} vs. ε_{22} curves. By the same token, Fig. 12 explains why the

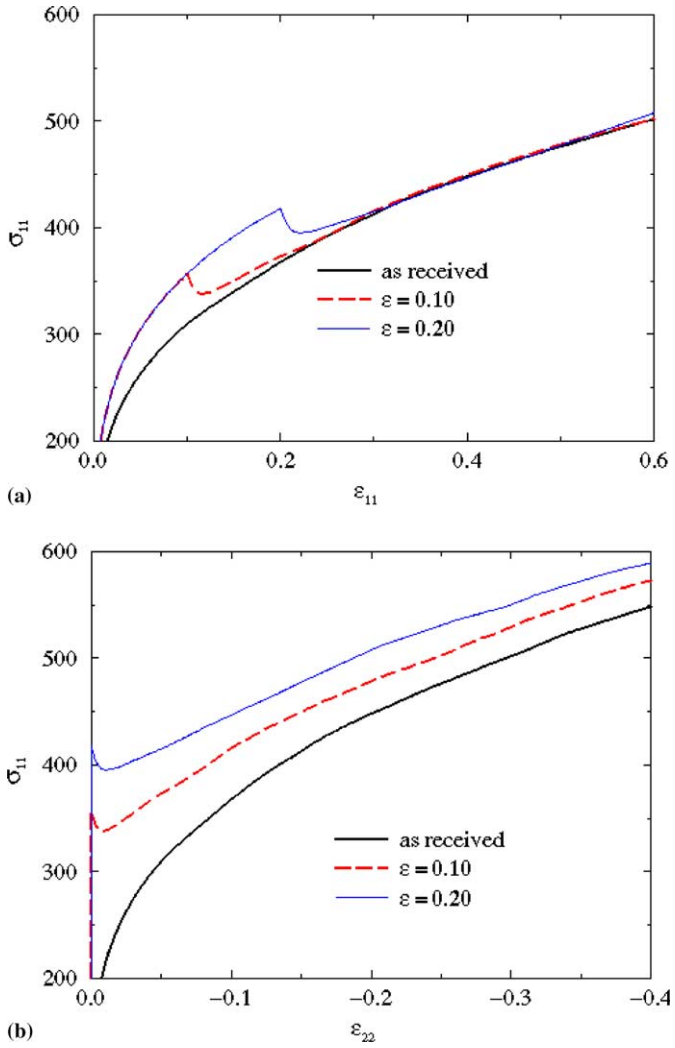

Fig. 11. Calculated σ_{11} vs. ε_{11} curves (a) and σ_{11} vs. ε_{22} curves (b) under uniaxial stretching after the sheet is pre-strained to different levels in in-plane plane strain tension ($\rho = 0$).

pre-straining significantly increases the limit strain ε_{11} but decreases the limit strain ε_{22} for equi-biaxial tension. However, it must be pointed out that, although the trend of in-plane plane strain pre-straining on forming limits is picked up quite well by mapping the FLSD, the pre-straining effect is overestimated by the mapping approach, especially for strain paths near equi-biaxial stretching ($\rho = 1$). It is found that the FLSc changes significantly near $\rho = 1$ (Fig. 5). It is also evident that the limit stresses for strain paths $\rho \approx 1$ for the sheets pre-strained in in-plane plane strain tension are below the FLSDs from linear strain paths. These observations could be used to explain why the mapping approach overestimates the limit strains in strain paths $\rho \approx 1$ for the pre-strained sheets.

Fig. 13 shows the effect of equi-biaxial tension ($\alpha = 1$) pre-straining on the FLD. As expected, the FLD is shifted towards the right because $\varepsilon_{22} > 0$ during the pre-straining. It is found that the pre-straining tends to decrease the limit strain ε_{11} for uniaxial stretching as can be estimated from Fig. 14, which gives the effect of

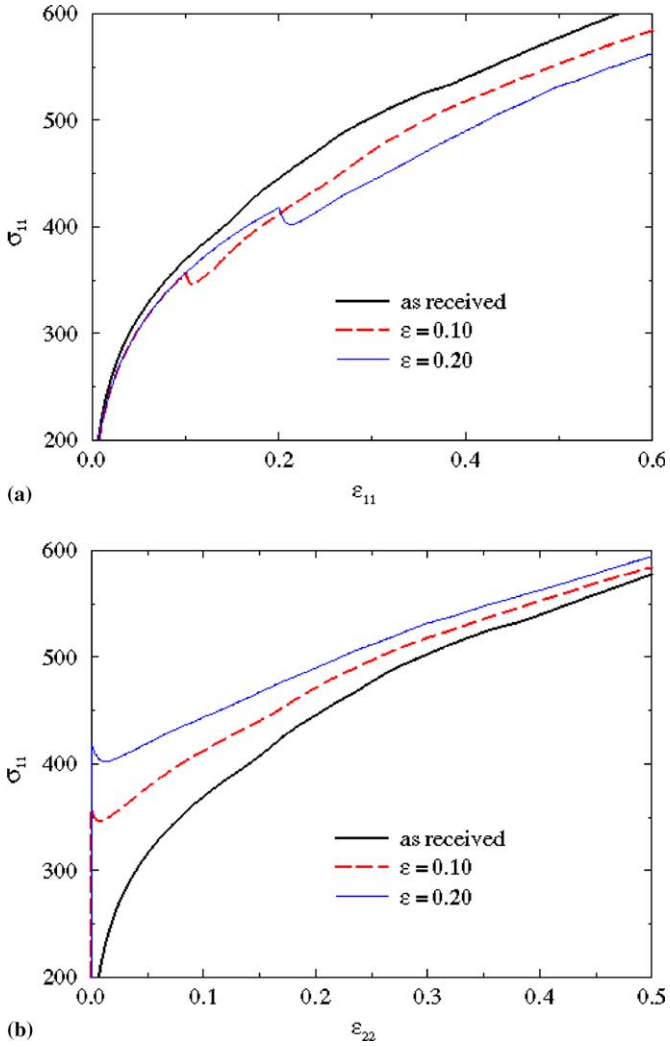

Fig. 12. Calculated σ_{11} vs. ε_{11} curves (a) and σ_{11} vs. ε_{22} curves (b) under equi-biaxial stretching after the sheet is pre-strained to different levels in in-plane plane strain tension ($\rho = 0$).

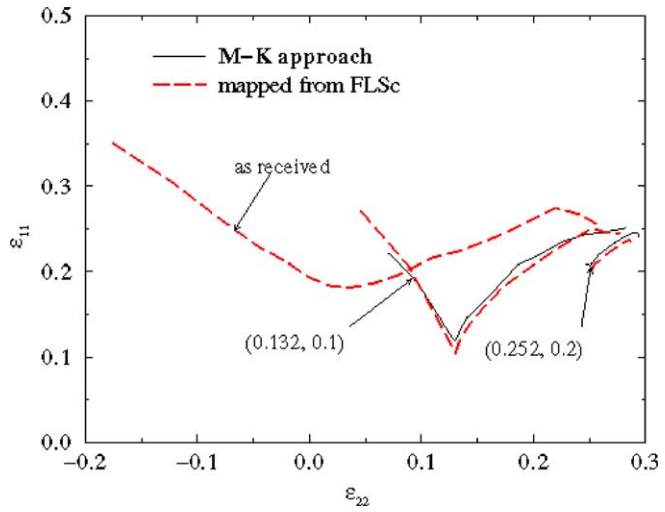

Fig. 13. Predicted FLDs for the sheet pre-strained to different levels in equi-biaxial tension ($\alpha = 1$).

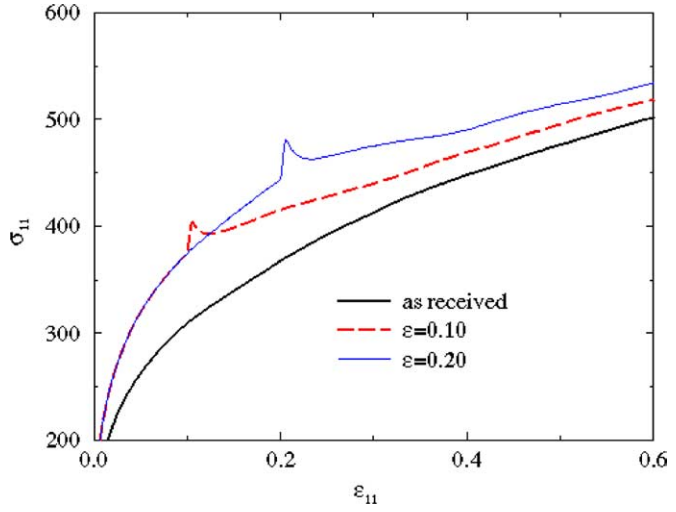

Fig. 14. Calculated σ_{11} vs. ε_{11} curves under uniaxial stretching after the sheet is pre-strained to different levels in equi-biaxial tension ($\alpha = 1$).

equi-biaxial tension ($\alpha = 1$) pre-straining on the response of uniaxial stretching in terms of the σ_{11} vs. ε_{11} curve. Furthermore, the limit strain ε_{11} for in-plane plane strain tension is decreased because the pre-straining increases the flow stress σ_{11} in subsequent in-plane plane strain tension as shown in Fig. 15. It is interesting to note that, even for the worst case, the FLD obtained by mapping the FLSD is still close to the one based on the M–K approach, although the limit stresses are noticeably above the FLSD (see Fig. 6b). We will return to this worst case later.

So far, the effect of strain path changes on the FLD has been studied by combining two linear deformation paths without unloading after the first strain path. The unloading effect on the FLDs is presented in Fig. 16 for pre-straining up to $\varepsilon_{11} = 0.10$ in uniaxial stretching ($\rho = -0.5$) and in-plane plane strain tension

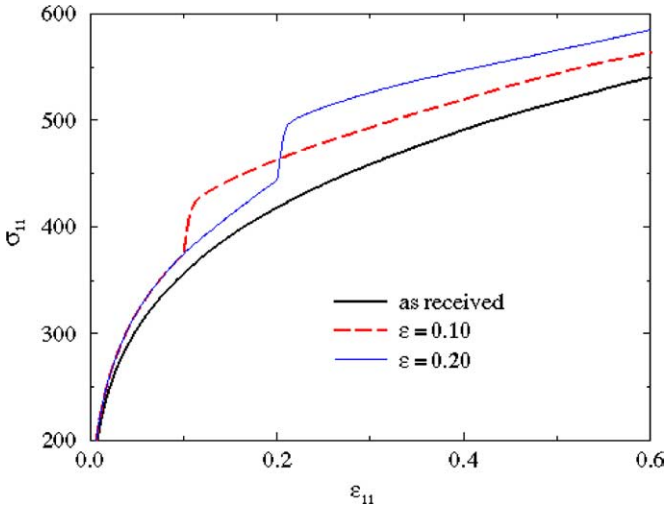

Fig. 15. Calculated σ_{11} vs. ε_{11} curves under in-plane plane strain tension after the sheet is pre-strained to different levels in equi-biaxial tension ($\alpha = 1$).

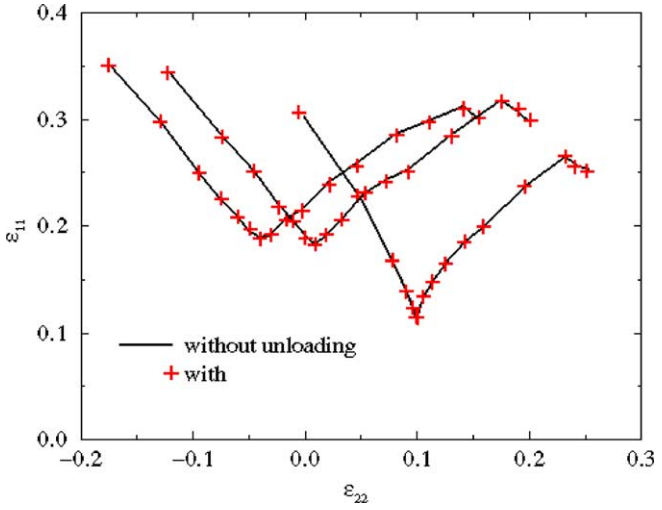

Fig. 16. Predicted FLDs for the pre-strained sheets with or without unloading after pre-straining to $\varepsilon_{11} = 0.1$ in uniaxial stretching, in-plane plane strain tension and equi-biaxial tension.

($\rho = 0$) as well as equi-biaxial tension ($\alpha = 1$). It is observed that the unloading has no noticeable influence on the forming limits for the level of pre-strain considered.

We have identified the worst case as being the sheet pre-strained in equi-biaxial tension ($\alpha = 1$) up to $\varepsilon_{22} = 0.252$ and $\varepsilon_{11} = 0.20$ (Fig. 6b). The calculated limit stresses based on the M–K approach were found to be well above the FLSD for linear strain paths. However, the FLD mapped from the FLSD was close to the one based on the M–K approach (Fig. 13). For the pre-strained sheet, the limit strains for uniaxial stretching are $(0.246, 0.206)$ based on the M–K approach and $(0.247, 0.210)$ by mapping the FLSD. It is noted that both of them are not very different from the strains $(0.252, 0.200)$, where the pre-straining

was terminated. In stress-space, the limit stresses in uniaxial stretching for the pre-strained sheet are (91.8, 473.7) and (375.3, 452.6) based on the M–K approach and the mapping from the FLSD, respectively. These limit stresses are quite different from each other, and are quite different to the stresses (441.8, 441.8) at the end of the pre-straining. However, it seems that the large difference in limit stresses between the M–K approach and the mapping approach does not result in a large difference in the corresponding limit strains. Perhaps, the reason for this is that the abrupt strain path change from equi-biaxial tension ($\alpha = 1$) to uniaxial stretching ($\rho = -0.5$) causes an immediately *intrinsic unloading*. This assumption of unloading due to an abrupt path change can be verified by comparing the von Mises effective stress $\sigma_e = \sqrt{\sigma_{11}^2 + \sigma_{22}^2 - \sigma_{11}\sigma_{22}}$ at the end of the pre-straining and at necking. The effective stresses at necking are, respectively, 435.1 and 419.3 MPa based on the M–K approach and the mapping from the FLSD, while $\sigma_e = 441.8$ is obtained at the end of the pre-straining. If the sheet is isotropic, decreasing σ_e implies unloading in classic plasticity theory. Although the stresses change dramatically during this intrinsic unloading, changes in the corresponding strains should remain relatively small because the unloading is an elastic process.

5. Discussion and conclusions

In this paper, we have calculated both the FLD and FLSD based on crystal plasticity theory in conjunction with the M–K approach. The effects of strain path changes on forming limits have been studied by considering non-proportional loading histories, which were prescribed using combinations of two linear deformation paths.

Our numerical results have indicated that the FLD is very sensitive to strain path changes. The strain limits could be either raised or lowered depending on the nature of the strain path change. More specifically, pre-straining in uniaxial stretching/tension raised the limit strains for subsequent in-plane plane strain tension and equi-biaxial stretching, while pre-straining in in-plane plane strain tension increased the limit strains for all subsequent strain combinations, and pre-straining in equi-biaxial tension decreased the formability for most strain combinations. Unfortunately, experimental results on the strain path changes were not available for the sheet considered in the present paper. However, the general trends of effects of strain path changes on forming limits are quite similar in steel and aluminium sheets (Laukonis and Ghosh, 1978; Graf and Hosford, 1994), and are predicted well by the M–K approach and by mapping directly from the FLSD.

The present study has confirmed numerically that, at least in comparison to the FLD, the FLSD is *not* sensitive to strain path changes. More specifically, the FLSD is almost path-independent when the pre-straining is not very large (Fig. 6a). Therefore, the calculated limit stresses under proportional loading paths could be used as the Forming Limit Stress curve (FLSc or simply FLSD) for the sheet. It has been demonstrated that the effects of path changes on FLDs revealed by the M–K approach could be reasonably reproduced by directly mapping the FLSD (Figs. 7, 10 and 13). In the case where the pre-straining is so large that it almost reaches the forming limit strain, the limit stresses are noticeably different from the FLSD calculated assuming linear deformation paths (Fig. 6b). However, even this large difference in stresses does not necessary result in a poor agreement in the FLD between the M–K approach and the mapping approach (Fig. 14).

We have also demonstrated that the nature of the effect of a strain path change on FLDs could be best understood by examining stress–strain curves and their intersections with the FLSD in some detail. For example, the decrease of the uniaxial ductility of the sheet due to biaxial pre-straining arises from increases in the flow stress σ_{11} under biaxial tension, resulting in a premature intersection with the FLSD when the deformation mode is changed from biaxial tension to uniaxial stretching (Fig. 13).

In summary, the FLD and FLSD are two mathematically equivalent representations of forming limits in strain-space and stress-space, respectively. However, the FLSD is much less path-dependent than the FLD

is. The investigation presented in this paper suggests that the FLSD is much more favourable than the FLD in representing forming limits in the numerical simulation of sheet metal forming processes.

Acknowledgement

The authors are grateful to Alcan International Limited for allowing the publication of this work.

References

Arrieux, R., 1995. Determination and use of the forming limit stress diagrams in sheet metal forming. Journal of Materials Processing Technology 53, 47–56.

Arrieux, R., Bedrin, C., Boivin, M., 1982. Determination of an intrinsic forming limit stress diagram for isotropic metal sheets. In: Proceedings of the 12th Biennial Congress IDDRG, pp. 61–71.

Asaro, R.J., Needleman, A., 1985. Texture development and strain hardening in rate dependent polycrystals. Acta Metallurgical 33, 923–953.

Graf, A., Hosford, W.F., 1993. Effects of changing strain paths on forming limit diagrams of Al 2008-T4. Metallurgical Transactions A 24, 2503–2512.

Graf, A., Hosford, W.F., 1994. The influence of strain-path changes on forming limit diagrams of Al 6111 T4. International Journal of Mechanical Sciences 36, 897–910.

Haddad, A., Arrieux, R., Vacher, P., 2000. Use of two behaviour laws for the determination of the forming limit stress diagram of a thin steel sheet: results and comparisons. Journal of Materials Processing Technology 106, 49–53.

Hecker, S.S., 1975. Formability of aluminum alloy sheet. Journal of Engineering Materials and Technology 97, 66–73.

Hill, R., 1948. A theory of the yielding and plastic flow of anisotropic metals. Proceedings of the Royal Society of London Series A—Mathematical, Physical and Engineering Science 193, 281–297.

Hiwatashi, S., Van Bael, A., Van Houtte, P., Teodosiu, C., 1998. Prediction of forming limit strains under strain-path changes: application of an anisotropic model based on texture and dislocation structure. International Journal of Plasticity 14, 647–669.

Hosford, W.A., 1979. On yield loci of anisotropic cubic metals. In: Proceedings of the 7th North American Metalworking Conference, SME, Dearborn, MI, pp. 191–197.

Janssens, K., Lambert, F., Vanrostenberghe, S., Vermeulen, M., 2001. Statistical evaluation of the uncertainty of experimentally characterised forming limits of sheet steel. Journal of Materials Processing Technology 112, 174–184.

Knockaert, R., Chastel, Y., Massoni, E., 2002. Forming limits prediction using rate-independent polycrystalline plasticity. International Journal of Plasticity 18, 231–247.

Kuroda, M., Tvergaard, V., 2000. Effect of strain path change on limits to ductility of anisotropic metal sheets. International Journal of Mechanical Sciences 42, 867–887.

Laukonis, J.V., Ghosh, A.K., 1978. Effects of strain path changes on the formability of sheet metals. Metallurgical Transactions A 9, 1849–1856.

Marciniak, Z., Kuczynski, K., 1967. Limit strains in the processes of stretch-forming sheet metals. International Journal of Mechanical Sciences 9, 609–620.

Neale, K.W., Chater, E., 1980. Limit strain predictions for strain-rate sensitive anisotropic sheets. International Journal of Mechanical Sciences 22, 563–574.

Stoughton, T.B., 2000. A general forming limit criterion for sheet metal forming. International Journal of Mechanical Sciences 42, 1–27.

Stoughton, T.B., Zhu, X., 2004. Review of theoretical models of the strain-based FLD and their relevance to the stress-based FLD. International Journal of Plasticity 20, 1463–1486.

Wu, P.D., Neale, K.W., Van der Giessen, E., 1996. Simulation of the behaviour of FCC polycrystals during reversed torsion. International Journal of Plasticity 12, 1199–1219.

Wu, P.D., Neale, K.W., Van der Giessen, E., 1997. On crystal plasticity FLD analysis. Proceedings of the Royal Society of London Series A—Mathematical, Physical and Engineering Science 453, 1831–1848.

Wu, P.D., Neale, K.W., Van der Giessen, E., Jain, M., Makinde, A., MacEwen, S.R., 1998a. Crystal plasticity forming limit diagram analysis of rolled aluminum sheets. Metallurgical and Materials Transactions A 29, 527–535.

Wu, P.D., Neale, K.W., Van der Giessen, E., 1998b. Effects of strain paths on sheet metal limit strains. In: de Borst, R., van der Giessen, E. (Eds.), Materials Instabilities in Solids. John Wiley & Sons Ltd., Chichester, pp. 243–253.

Wu, P.D., Graf, A., Jain, M., MacEwen, S.R., 2000. On alternative representation of forming limits. Key Engineering Materials 177–180, 517–522.

Wu, P.D., Jain, M., Savoie, J., MacEwen, S.R., Tugcu, P., Neale, K.W., 2003. Evaluation of anisotropic yield function for aluminum sheets. International Journal of Plasticity 19, 121–138.

Zhao, L., Sowerby, R., Sklad, M.P., 1996. A theoretical and experimental investigation of limit strains in sheet metal forming. International Journal of Mechanical Sciences 38, 1307–1317.

Zhou, Y., Neale, K.W., 1995. Predictions of forming limit diagrams using a rate-sensitive crystal plasticity model. International Journal of Mechanical Sciences 37, 1–20.

Zimniak, Z., 2000. Implementation of the forming limit stress diagram in FEM simulations. Journal of Materials Processing Technology 106, 261–266.